

Soft Matter

Accepted Manuscript



This is an *Accepted Manuscript*, which has been through the Royal Society of Chemistry peer review process and has been accepted for publication.

Accepted Manuscripts are published online shortly after acceptance, before technical editing, formatting and proof reading. Using this free service, authors can make their results available to the community, in citable form, before we publish the edited article. We will replace this *Accepted Manuscript* with the edited and formatted *Advance Article* as soon as it is available.

You can find more information about *Accepted Manuscripts* in the [Information for Authors](#).

Please note that technical editing may introduce minor changes to the text and/or graphics, which may alter content. The journal's standard [Terms & Conditions](#) and the [Ethical guidelines](#) still apply. In no event shall the Royal Society of Chemistry be held responsible for any errors or omissions in this *Accepted Manuscript* or any consequences arising from the use of any information it contains.

Coarse-grained simulation of dynamin-mediated fission[†]

Marc Fuhrmans^a and Marcus Müller^{*a}

Received Xth XXXXXXXXXXXX 20XX, Accepted Xth XXXXXXXXXXXX 20XX

First published on the web Xth XXXXXXXXXXXX 200X

DOI: 10.1039/b000000x

Fission is a process in which a region of a lipid bilayer is deformed and separated from its host membrane, so that an additional, topologically independent compartment surrounded by a continuous lipid bilayer is formed. It is a fundamental process in the organization of the compartmentalization of living organisms and carefully regulated by a number of membrane-shaping proteins. An important group within these is the dynamin family of proteins that are involved in the final severance of the hourglass-shaped neck, via which the growing compartment remains connected to the main volume until the completion of fission. We present computer simulations testing different hypotheses of how dynamin proteins facilitate fission by constriction and curvature. Our results on constraint-induced fission of cylindrical membrane tubes emphasize the importance of the local creation of positive curvature and reveal a complex picture of fission, in which the topological transformation can become arrested in an intermediate stage if the proteins constituting the fission machinery are not adaptive.

1 Introduction

The separation of an inside from an outside lies at the very heart of cellular life, and the organization of living organisms into cells and sub-cellular compartments is required for a large number of biological functions. This compartmentalization is maintained by lipid bilayers and undergoes frequent but carefully regulated topological changes. One of these changes is membrane fission, during which a continuous region of space surrounded by a lipid bilayer is divided, creating an additional topologically disconnected compartment in the process. Usually, the topological change is preceded by a morphological preparation, in which the bilayer region about to be sealed off is arranged into an invaginated pit or a protruding bud that only remains connected to the main volume via a narrow, hourglass-shaped neck¹.

While this morphological preparation can be considered part of the fission process and is definitely a necessary step, in this article we are going to reserve the term ‘fission’ for the proper topology-changing part of the process only, i.e. the transition from a continuous hourglass-shaped region of a lipid bilayer to two separate bilayers facing each other. Like its reverse, the fusion process, the intermediate stages of this process will involve energetically unfavorable geometries^{2–5}, and it will be necessary to either provide mechanical work or to substantially deform or perturb the lipid bilayer before the topological transition will take place spontaneously (cf. ref.⁶ for a recent review).

For fission, this role is believed to be filled by the dynamin

family of proteins, which has been proven to be essential for fission in endocytosis^{7–9}. In the cytosol, these large GTPases occur as tetramers^{10,11}, but they can spontaneously polymerize into helical assemblies^{12,13}, particularly upon binding to tubular regions of lipid bilayer, e.g. the neck of a clathrin-coated pit¹⁴. Additionally, these helical complexes have been shown to undergo a conformational change upon addition of GTP, in which the turns of the helix move relative to each other^{15,16}, causing simultaneous constriction, elongation and twisting of the spiral. Each of these modes of movement has been proposed to be individually responsible for fission, giving rise to a ‘constrictase’ model¹⁵, a ‘popase’ model¹⁷ and a ‘twistase’ model¹⁸, as well as combinations of these models^{18,19}.

It was, however, criticized that these large extended helical structures only form in the absence of GTP, whereas the continuous presence of GTP under physiological conditions would prevent the formation of assemblies larger than the minimum size required to enhance the GTPase activity²⁰, and the onset of GTP hydrolysis upon reaching that threshold size^{10,21} would cause disassembly of the complex²². Moreover, the extended dynamin complexes formed in the absence of GTP were found to stabilize narrow bilayer tubules of radii below the threshold at which they would break in the absence of dynamin²³, casting doubt on mechanisms primarily based on constriction. Instead, a model, in which several assembly and disassembly cycles of dynamin occur before fission, has been proposed explaining the observed stochastic variation of fission times²², and the change in curvature stress by desorption of dynamin potentially triggers the topological change²³.

The role of curvature stress has also been emphasized in another study focusing on the details of the pleckstrin homology

[†] Electronic Supplementary Information (ESI) available: [details of any supplementary information available should be included here]. See DOI: 10.1039/b000000x/

(PH) domain²⁴, which acts as the membrane anchor of dynamin. This PH domain possesses several hydrophobic loops, which are expected to shallowly penetrate into the tail region of the lipid bilayer^{25–27}, as well as a binding pocket with a high affinity for negatively charged lipids²⁸, which could potentially cause a lipid to protrude from the membrane, dragging along its surroundings. Both this deformation and the additional volume introduced at the periphery of the tail region by the hydrophobic loops give rise to a positive spontaneous curvature, which conflicts with the negative curvature of the constriction's geometry but which may potentially be resolved by further reduction of the tubule radius at a distance from the PH domains' location. Such a reduction will create a positive curvature at the location of the PH domain–lipid interaction, especially when neighboring turns of the dynamin complex are free to tilt and cooperatively profit from the generated contraction in their middle²⁴.

Experimentally, it is difficult to resolve the pathway of topological changes and the involvement of dynamin. One either needs to freeze the process in time by using unhydrolyzable GTP analogs to allow for a structural analysis (e.g. ref.²⁹), or one relies on indirect methods like conductance measurements to deduce information about the fission mechanism (e.g. ref.²³). Computer simulations using coarse-grained models, on the other hand, can access the necessary system sizes and time scale to resolve the process at molecular resolution. Moreover, it is possible to use idealized models in simulations that one can specifically tailor to study the effects of an isolated factor or to test a proposed hypothesis, which would be much harder in an experimental setup.

In this article, we employ such a simulation approach that aims at investigating universal aspects of dynamin-mediated membrane fission. For the lipids, we use a coarse-grained, solvent-free lipid model^{30,31} that has been shown to accurately represent important characteristics of lipid bilayers like area per lipid, membrane thickness, and elastic properties, as well as complex collective phenomena like phase transitions, dynamic properties^{30,32} and topological changes³¹. Therefore we expect to capture the factors relevant to fission. With this model, we represent the narrow membrane neck, which will be cleft in the fission process, by a cylindrical bilayer tube. In the same spirit, we do not use an atomistic representation of the dynamin complex but also employ a more idealized, coarse-grained representation. Rather than trying to create a detailed model of the dynamin complex in an attempt to match all known properties simultaneously, we isolate the different effects of dynamin and study their influence on our system independently. We use two coarse-grained representations of the PH-domain in order to test the system's response to constriction and the role of curvature induced by the interaction with the PH domains.

Specifically, we use a cuff-shaped repulsive potential to test

the system's response to constriction, which we present in the first half of Section 3, before we switch to a representation of the dynamin complex that explicitly includes the membrane-interacting PH domains as amphiphilic disks using a particle-based description. By restraining these disks to their expected relative positions using simple harmonic potentials, we study the effects of shallow membrane insertion and the concomitant local creation of curvature in addition to constriction. Our results emphasize the importance of the creation of local curvature by the membrane-binding domains, which greatly reduces the necessity of creating a protein scaffold with a very small radius. In addition, we find that different steps of the fission process have incompatible requirements, and the topological transition can become arrested in an intermediate stage if the proteins constituting the fission machinery are not adaptive.

2 Coarse-grained model and simulation methods

2.1 Scope of the simulations

Before we go into the discussion of our results, it is important to establish some common ground on the kind of conclusions that can be drawn from the data obtained with our simulations. For this, there are two factors which need to be addressed: the lipid model used, and the even more idealized representation of dynamin.

Coarse-grained lipid models, like the one used in our simulations, have become a well established tool in the study of collective phenomena in lipid bilayers^{33–35}. On the one hand, the difficulty of direct experimental observations of the transient states in topological changes like fission and fusion that occur on the nm- and μ s-scale makes it necessary to resort to calculations and computer simulation to deduce the details of these structures. On the other hand, a detailed, atomistic representation of the large number of lipids involved in these collective phenomena for the necessary timescales in a simulation is computationally very expensive and not possible at present. Luckily, the universality of the behavior of lipids lends itself to coarse-grained representations, in which less relevant degrees of freedom are integrated out³³, but the behavior of lipid bilayers is still accurately captured. As such, the model used in our simulation was shown to reproduce elastic properties³⁰ as well as complex phenomena like phase behavior³⁰, topological transitions³¹ and dynamic properties³². Considering these aspects of lipid behavior the most relevant to fission, we argue that the response of lipid bilayers to external disturbances observed in our simulations are indicative of what may occur on the molecular level in-vivo and in-vitro.

In the same spirit, we simplify the representation of the dynamin complex in our model, and only include selected properties that have been discussed in connection to fission. This

way, we can directly study the influence of these aspects on the lipid bilayer and even emulate hypothetical scenarios, in which only a subset of the factors associated with real peptides are considered. The aspects we consider are the exertion of constricting forces on cylindrical bilayers and small vesicles^{15,16}, and the shallow insertion of domains of dynamin and other proteins relevant in fission into the lipid bilayer^{24–26,36}. In our simulations, we implement these factors with a constricting, repulsive potential, and with the insertion of amphiphilic disks constrained to a certain location via harmonic potentials. While these representations were inspired by experimental findings on dynamin, our aim is to study how the lipids react in response to the introduced disturbance. Our conclusions will therefore be of a general nature, and the different modes of action we consider for the proteins constituting the fission machinery should not be seen as necessarily appertaining to a specific protein like dynamin, but may just as well be relevant to other involved peptides like, e.g., the BAR domain family of proteins³⁶. In addition, while the local curvature in our simulations was created entirely by shallow insertion, our observations of the curvature's effects can be considered largely independent on the manner in which the curvature was created, and may just as well apply to more specific modes of curvature generation like, e.g., a lipid binding pocket^{24,28}.

2.2 Lipid model

We used a coarse-grained, solvent-free model of lipid bilayers^{30,31,37} to study the topological changes involved in fission of cylindrical lipid bilayers. A lipid molecule is represented by a linear chain consisting of two polar head-group beads and eight hydrophobic tail beads that are tethered by harmonic bond potentials and a simple bond-angle potential. Non-bonded interactions are defined via a weighted-density functional of the bead densities. This model accurately captures the relevant characteristics of lipid bilayers and has previously been used to study the liquid-gel transition³⁰, collective bilayer dynamics³², as well as the mechanisms of spreading of vesicles on hydrophilic surfaces³¹.

The specific interaction parameters were chosen so that the lipids self-assemble into the lamellar phase (planar bilayers) at equilibrium. A detailed compilation of the model parameters can be found in ref.³¹ along with a general description of the behavior of our model. We use the thermal energy $k_B T$ as unit of energy, the range of the non-bonded interactions, σ , as unit of length, and denominate the unit of time as τ . The bilayer thickness d_{HG} , defined as the separation of the head-group peaks of the density profile across the bilayer membrane, has a value of $d_{HG} = 4.30 \sigma$ in our model. Using d_{HG} and the lateral self-diffusion coefficient $D = 0.013 \sigma^2 / \tau$ of a lipid in a planar membrane, we can establish a relation between our model and

experimental properties of biologically relevant lipid systems. This mapping yields the correspondences of $1 \sigma \approx 0.9 \text{ nm}$ and $1 \tau \approx 2 \text{ ns}$ ³¹.

2.3 Cylindrical bilayers

Cylindrical tubes of lipid bilayers were explicitly arranged. We started with numbers of lipid molecules in the inner and outer monolayer that were estimated by ring the respective areas of the monolayers. The initial numbers in the monolayers, however, are not crucial, because in simulations in the $NP_x T$ ensemble, the cylinder can freely elongate or shorten, changing its radius to a value that suits the chosen lipid distribution.

A change of the constriction radius additionally gives rise to an areal density difference between the two monolayers. In the experiment, this difference can be relaxed by exchanging lipids between the constricted region and the connected free membrane reservoir on both sides of the constricted neck. In the finite-sized simulation cell, this areal density difference is only partially relaxed by repartitioning of lipids between the constricted and free membrane and the concomitant changes in cylinder radius, length of the simulation cell, or areal densities. However, even in the absence of flip-flop events, we do not expect this effect to introduce significant artifacts because the relaxation of the areal density difference can be accommodated by movement of a few lipid molecules.

We used a system with an equilibrium radius of 6.9σ , an average length of 21.5σ , and a total number of 3600 lipids with an inside-to-outside ratio of 126:205. A plot of the radial distribution of the bead density in our system is shown in Fig. 1. It should be noted, however, that on a timescale allowing lipid exchange between the monolayers, the equilibrium radius would go towards infinity. In addition, we created a larger system by duplicating the original system along the cylinder axis. We used the latter system for simulations that incorporate multiple rings of peptide disks.

2.4 Cuff potential

In the first set of simulations we employ a minimal representation of the dynamin complex that is capable of constricting the bilayer tube. A cuff potential describes the repulsive interactions between the lipids in the cylindrical lipid bilayer and the atoms in the dynamin complex. This cuff potential is defined around a cylindrical mantle and, principally, takes the form of a Lennard-Jones 9-3 potential,

$$V_{9-3}(d) = C \times (d^{-9} - d^{-3}). \quad (1)$$

In our simulations we use a potential strength $C = 10.0 k_B T$. The potential is cut off and shifted to zero at the minimum. Therefore the cuff potential only gives rise to repulsive forces,

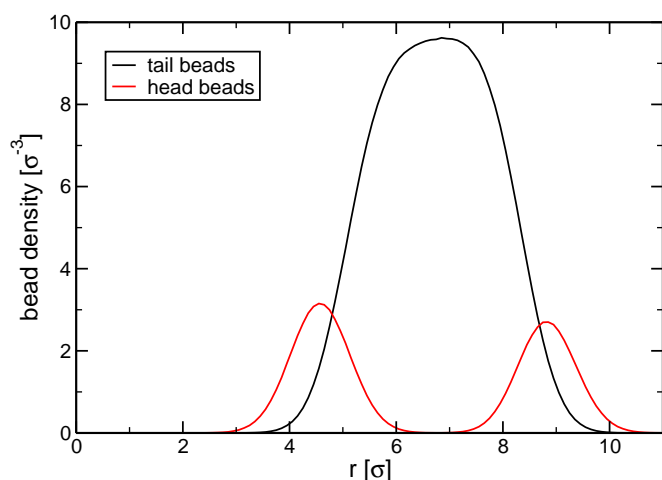


Fig. 1 Bead density as a function of the distance, r , to the cylinder axis for the equilibrated cylindrical lipid bilayer.

which always act perpendicular to the mantle. This is accomplished by considering the closest point on the cylinder mantle as reference to determine the distance, d , which is used to compute the force. The direction of the force is always originating from that closest point and therefore pushes the particle away from the cylindrical mantle. To avoid too large forces that might occur during system setup or from the relatively large integration step of the coarse-grained model, we also truncated the force below a distance of 1.11σ by replacing the Lennard-Jones potential by linear extrapolation. Fig. 2 gives a schematic representation of the cuff geometry and presents the potential and concomitant force.

The radius of the cylindrical reference was either held constant during the simulations or dynamically changed with time in the course of the simulations. In the latter case, we introduced a minimum radius of 3.0σ , beyond which the radius could not be reduced.

2.5 Peptide model

In the second set of simulations we endow the coarse-grained model of the dynamin complex with additional molecular details that mimic the flexibility and shallow insertion of the PH domains. The peptide model uses the same two particle types as the lipid model – hydrophilic and hydrophobic beads. Rather than including the entire dynamin complex, however, we only added the peptides that represent the PH domains, and explicitly restrained these to positions corresponding to their location in the polymeric assembly using harmonic potentials. For simplicity, we modeled the PH domain as a hexagonal amphiphilic disk with one layer of polar beads and one layer of apolar beads.

The peptides' shape was maintained by a network of har-

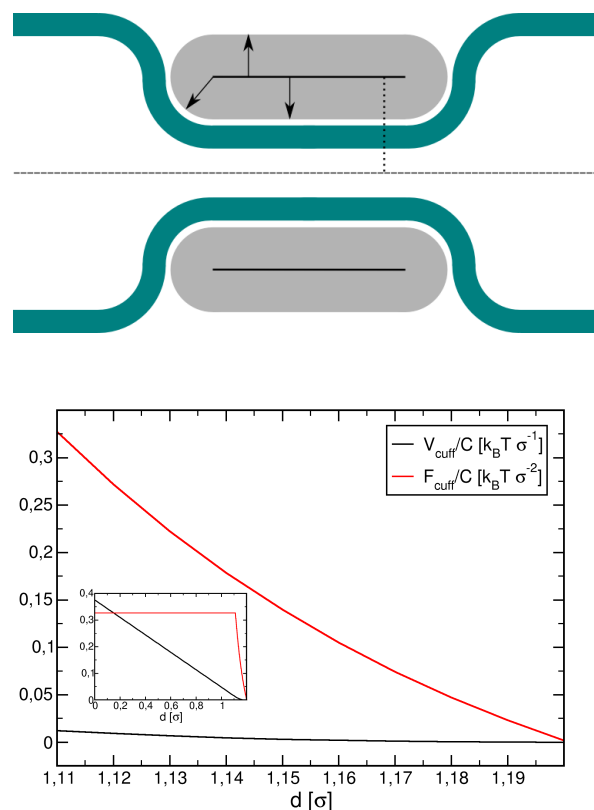


Fig. 2 (top) Schematic 2D representation of the cuff potential. The cylindrical reference is indicated by the bold black lines, and the gray shaded area corresponds to the range of the potential. Arrows illustrate the direction of the resulting forces for different positions, and the dotted line indicates the cuff radius. The green shape represents the cylindrical lipid bilayer and its constriction by the cuff potential. (bottom) Plot of the potential and the corresponding force. The potential is cut off at the minimum, and the force is truncated for distances smaller than 1.11σ . The main plot shows the range beyond 1.11σ , whereas the inset also shows the linear extrapolation used for small distances.

monic bonds with a stiff force constant of $2000k_B T \sigma^{-2}$, which restrained fluctuations of the distance between nearest neighbors within the disks as well as the distance between the two apposing disks around 0.7σ . Fig. 3 gives an illustration of the peptides. We used 3 beads per edge of the hexagonal disks, resulting in an edge length of 1.4σ and a disk “diameter” of 2.8σ . In simulations where the peptides' center of mass was restrained to fixed coordinates, a harmonic potential with a force constant of $5k_B T \sigma^{-2}$ was used.

In order to reflect the variability of the hydrophobic binding loops of the PH domain, we used a bead density corresponding to the average area density of lipid head-groups in an unperturbed bilayer, which means that with the soft inter-

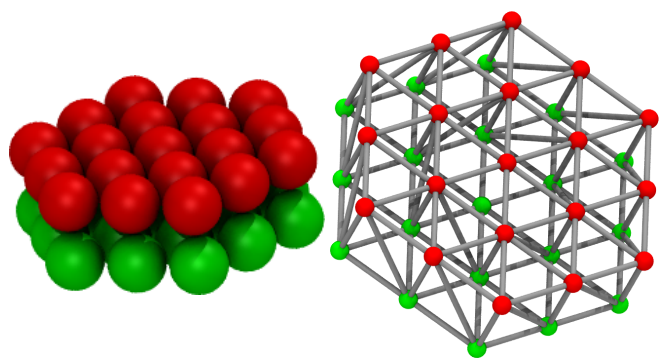


Fig. 3 (left) The hexagonal disks representing the dynamin complex in our coarse-grained model. (right) Visualization of the network of harmonic bonds used to keep the peptide's shape.

actions of our coarse-grained models lipids and peptides can still overlap. Fig. 4 gives plots of the peptides' effect on the lipid bead density in a planar bilayer, showing that the head-group density in the affected monolayer drops to roughly half of the unperturbed value, whereas the tail bead density is reduced by a lesser amount. With the tail beads, one can also observe a packing effect with a spacing that corresponds to the arrangements of particles in our amphiphilic disks.

2.6 Simulation method and setup

We use molecular dynamics simulations with a dissipative particle dynamics (DPD) thermostat^{30,38,39} The simulations of cylindrical lipid bilayers were performed in an ensemble, in which the pressure along the cylinder axis, the x -axis, was held constant at zero (NP_xT ensemble). For simulations of planar bilayers, we used a similar ensemble in which the tangential pressure was held at zero (NP_T).

The details of the simulation method have been previously presented³⁰, and the simulation parameters are identical to those used in our study of vesicle spreading in ref.³¹, i.e. an integration step of 0.005τ , and a friction coefficient of 0.5 for the DPD thermostat along with a mass of 0.0001 and a friction coefficient of 0.1 for the additional degree of freedom representing the fluctuations of the box dimensions in the NP_xT and NP_T ensembles.

The different setups of simulations reported in this article are compiled and compared in Fig. 5. All simulations have in common that a cylindrical lipid bilayer is used. In the simulations using a cuff potential, panel A, a repulsive potential defined around a cylindrical reference around the cylindrical bilayer is used to constrict the membrane. In the simulations using amphiphilic disks to represent the PH domains of the dynamin complex, the disks' centers of mass are restrained to positions spaced evenly along a ring around the lipid tube. Apart from simulations using only a single ring of peptide

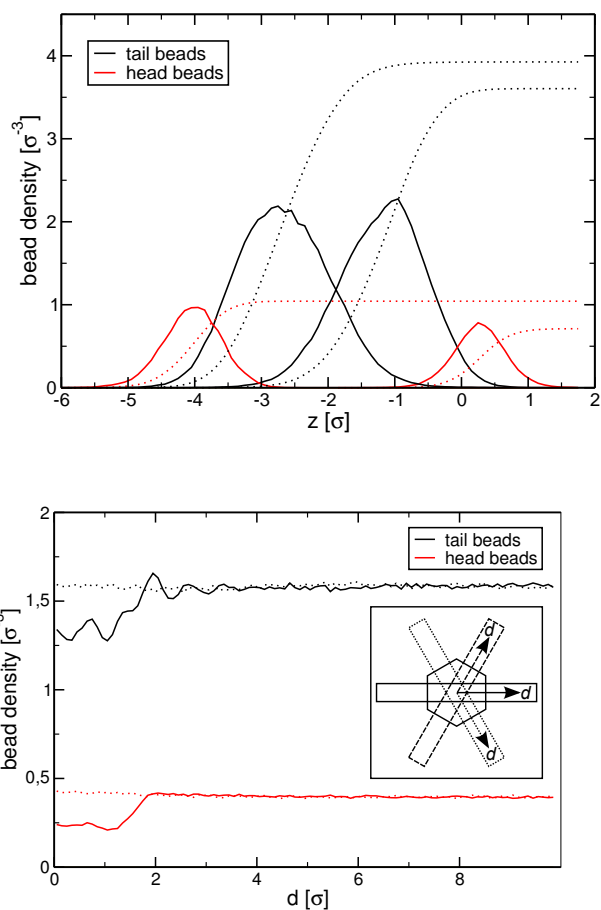


Fig. 4 Profiles of the bead density of lipids in a planar bilayer, in which a single amphiphilic disk is embedded. (top) Bead density within a circular area with radius 2σ around the amphiphilic disk embedded at the lipid/water interface. The densities are divided according to the leaflet the lipids originate from, and integrals of the peaks are plotted as dotted lines for comparison. The center of mass of the peptide disk lies at $z = 0\sigma$. (bottom) Lipid bead density in a volume slice perpendicular to the lipid bilayer. The volume slice is centered around the plane cutting the hexagonal amphiphilic disk in half so that the intersection runs through the middle of opposing edges of the hexagon and it is thin enough so that the entire volume slice lies within the intersected edge, as illustrated by the three rectangles in the inset. In addition to the proximal monolayer interacting with the peptide disk, dotted lines show the density profile of the distal monolayer.

disks, we also performed simulations with two single rings around the bilayer (Fig. 5 B), and simulations in which the single rings were replaced with double-rings (Fig. 5 C). These double-rings consist of two rings placed next to each other with a very small separation – typically 0.5σ – allowing us to control the curvature by assigning different radii to the sub-

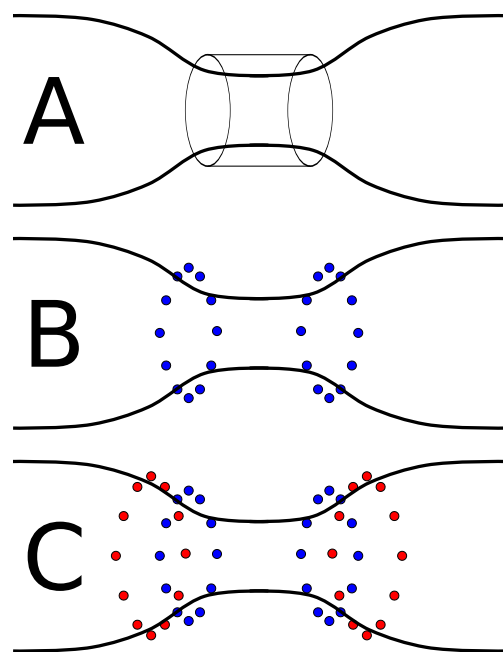


Fig. 5 Overview of the different setups of simulations. A: Constriction of the membrane tube using a repulsive cuff potential around the bilayer. By assigning different radii to the cylinder, we can constrict the bilayer tube. B: Two separated rings of disks that represent the PH domains of the dynamin complex. The peptide disks are restrained to anchor points, shown as colored circles in B and C, evenly spaced along a ring around the bilayer tube. C: Two double-rings of peptides exert more control on the curvature by assigning different radii to the two subunits of the double-rings.

units of the double-rings.

3 Results

3.1 Dynamin as cuff-shaped potential

We first study the effects of a single, isolated constriction. For this, we employed a repulsive cuff potential of length 2σ around the bilayer tube. We started at a cuff radius at which no lipids were within the potential's range and slowly reduced the cuff radius at a constant velocity of $0.001\sigma\tau^{-1}$. At this rate of tightening, it takes longer than 4000τ to decrease the cuff radius by a single bilayer thickness, giving the lipids ample time to relax with their self diffusion constant of $0.013\sigma^2/\tau$, and the system had time to relax the tension arising in the direction of the cylinder axis by increasing the corresponding box dimension via the pressure coupling. With this setup, we were able to observe the topological details of the fission process as well as to measure the free energy of the constriction up to the point at which topological changes occur. During the first part of the constriction, we observe a simple defor-

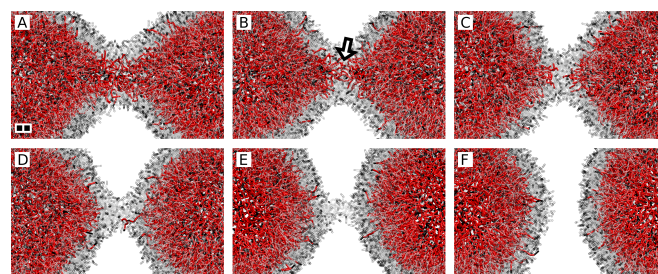


Fig. 6 Topological changes during fission caused by a constricting cuff potential. Head-group beads are shown in black, and tails belonging to the inner and outer monolayer in red and gray, respectively. Lipids from the outer monolayer have been rendered with reduced opacity to allow an unobstructed view on the topology of the inner monolayer. At first, there is still a continuous region of high head-group density running through the constricted region (A: 0τ). At some point, however, this region becomes discontinuous, and a gap appears, in which only tails from the lipids in the inner monolayer remain (B: 130τ). This rupture is marked by an arrow. From then onwards, the topology of the constriction gradually becomes wormlike-micelle-shaped, and lipids originating from the inner monolayer move out of the constricted region as the extended micelle topology grows (C: 270τ , D: 1200τ) until, at some point, the connection ruptures altogether (E: 1840τ) completing the fission process. The remaining dimples are absorbed into the bilayer (F: 1860τ). The patterned bar shown in the lower left of panel A corresponds to a distance of 2σ .

mation, in which the lipid bilayer tube becomes more narrow as it is “squeezed” by the cuff potential and assumes an hour-glass shape (see Fig. 20 / Electronic Supplementary Information (ESI)).

The subsequent topological changes are visualized in Fig. 6. At first, the lumen of the cylindrical bilayer closes. However, a region of high head-group density still connects the left and right sides of the membrane tube along the central axis, i.e. the bilayer topology still remains clearly separated into two distinguishable monolayers (Fig. 6 A). The first topological change takes place when the continuous connection of the head-groups ruptures (Fig. 6 B), and locally only lipid tails remain in the inner monolayer of the tube. The rupture location is marked by an arrow in panel B. Once this topological change has occurred, the lipids of the inner monolayer move away from the rupture location, and the topology of the connection gradually turns into a wormlike micelle. This morphology is the analog of the stalk – an important intermediate in membrane fusion. It persists for over 1000τ and only becomes thinner as the cuff potential constricts further as depicted in panels C and D. Eventually, as presented in panel E, the hydrophobic connection breaks after its diameter has been squeezed to almost half the thickness of an unperturbed bilayer. This second topological change completes the fission

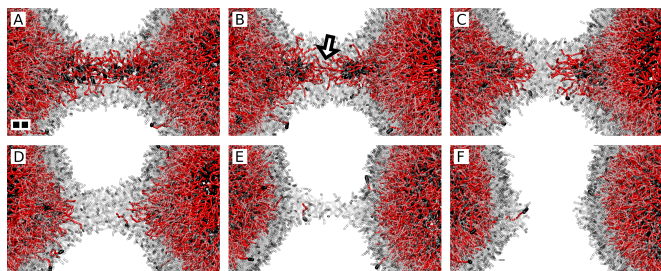


Fig. 7 Same as Fig. 6, except that a longer cuff with a length of 6σ was used. At first, there still remains a continuous region of high head-group density running through the constricted region (A: 0τ). The first topological change is associated with a local rupture (arrow) of this inner head-group connection (B: 110τ). Subsequent squeezing gradually pushes lipids, originating from the inner monolayer, out of the constricted region as the extended micellar topology grows (C: 230τ , D: 400τ). Later, the rupture of this hydrophobic connection completes the fission (E: 1800τ) and the membrane shape relaxes (F: 1830τ). The patterned bar in the lower left of A corresponds to a distance of 2σ .

process. Subsequently the remaining dimples are adsorbed into the bilayer.

Since the cuff potential used in Fig. 6 was too short to determine a preferred location of the topological changes, i.e. near to the edge of the constriction or close to its center, we repeated the simulations with a longer cuff potential of length 6σ . Fig. 7 shows the details of the topological changes for one out of a total of four simulations conducted for this extended cuff potential. We found the origin of the initial topological change, the rupture of the connecting head-group region, to lie within the central zone of the constriction and not directly at its edges.

Interestingly, also in the simulations with the spatially extended cuff potential, the wormlike-micelle topology persisted for over 1000τ , and only ruptured after the cuff potential had forced its diameter to reduce to almost half a bilayer thickness. Additionally, we performed three extended simulations at constant cuff radius, starting from the configurations depicted in Fig. 7 B, C and D. In all of these simulations, the fission process did not proceed beyond forming the wormlike micelle topology, which then persisted without further change for the complete 8000τ duration of the simulations.

The conformational change of the helical dynamin assembly does not only constrict the membrane tube but goes along with an elongation of the constricted region (a ‘popase’ model¹⁷). In order to test if an additional elongation of the cuff potential, on top of the constriction, will facilitate the rupture of the wormlike micelle, we have performed a series of simulations, in which we did not only reduce the cylinder radius of the cuff at the defined speed but simultaneously extended its length so that the area of the cylinder mantle re-

mained constant. Fig. 8 (and also Figs. 21 / Electronic Supplementary Information (ESI)) present the simulations with this setup. Topologically, the fission process proceeds along the two-step mechanism that is identical to what we observed with the non-elongating cuff potential and also the formation of the wormlike-micelle topology (first topological change) occurred at a similar cuff radius as in the systems with the non-elongating cuff potential. Importantly, however, the wormlike-micelle connection ruptured at significantly smaller constriction than before. For comparison, we also performed simulations with a non-elongating cuff while applying a tension of $0.01 k_B T \sigma^{-2}$ along the tube axis (x -direction), which gave results very similar to the simulations using an elongating cuff potential. Tab. 1 compiles an overview of the times and cuff radii, at which first topological change from a tube to a wormlike micelle is observed, i.e. the connectivity of the inner monolayer becomes broken, and the times, at which the hydrophobic connection is broken and fission is completed.

We also analyzed the locations of the topological changes in the simulations with the elongating cuff potential, and found that both the rupture of the inner monolayer as well as the rupture of the wormlike micelle did not occur directly at the very edge of the constricted region but rather somewhere along its length. Moreover, there was correlation between the location of the two topological changes within individual trajectories, i.e. for the three simulation runs, we observed a remarkable proximity between the points of rupture of the inner monolayer (wormlike-micelle formation) and the outer monolayer (fission). In fact, the two locations were almost identical, as shown in Fig. 9, which agrees with the rather short time span of less than 500τ between first local occurrence of a wormlike-micelle topology and final rupture (cf. Table 1).

In order to estimate the change in free energy involved in creating the constriction *before* topological changes occurred, we performed simulations at various, time-independent cuff radii using a 2σ long cylinder and recorded the average force, F_p , that the lipids exerted on the potential in the direction perpendicular to the cylinder axis and the average radius of the lipids located within the cylinder. Fig. 10 shows a plot of the results, as well as its integral, which corresponds to the free-energy change upon constriction.

We also recorded the average force per coarse-grained interaction center, $\langle f \rangle$ (see Fig. 22 / Electronic Supplementary Information (ESI)), and the average total force, $\langle F \rangle$ (cf. Fig. 11), exerted on the lipids as a function of the location along the cylinder axis for a wide and a narrow cuff potential. Since the force exerted by our potential is always positive and grows with increasing penetration into the potential (up to a truncated value), $\langle f \rangle$ is a measure of the depth of penetration of the lipid molecules. We find that, for a narrow cuff, the lipids experience the largest force at the periphery of the cuff, whereas the dependence is less pronounced for the wider cuff. $\langle F \rangle$,

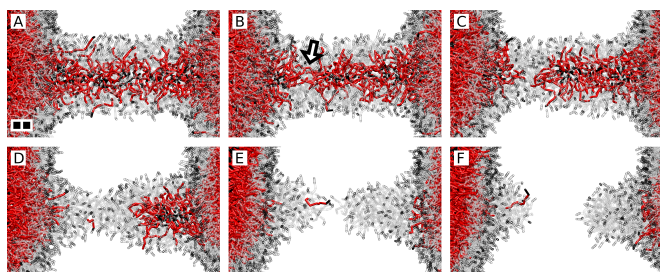


Fig. 8 Topological changes during fission caused by a constricting and simultaneously elongating cuff potential. Lipids from the outer monolayer have been rendered with reduced opacity to allow an unobstructed view on the topology of the inner monolayer. At first, there is still a continuous region of high head-group density running through the constricted region (A: 0τ). At some point, however, this region becomes discontinuous, and a gap appears (arrow mark), in which only tails from the lipids in the inner monolayer remain (B: 50τ). From then on, the topology of the constriction becomes more and more wormlike micelle shaped, and lipids originating from the inner monolayer move out of the constricted region as the extended micellar topology grows (C: 100τ , D: 200τ), until at some point the connection ruptures altogether (E: 310τ) and is absorbed into the bilayer (F: 320τ). The patterned bar shown in the lower left of A corresponds to a distance of 2σ .

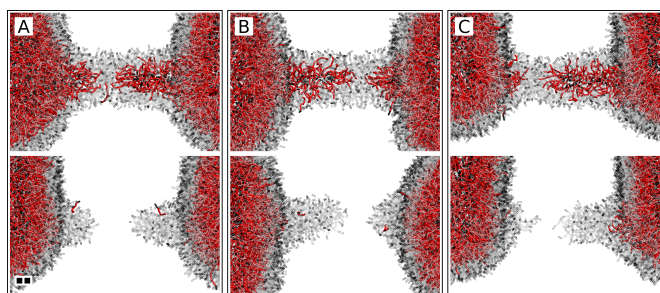


Fig. 9 Alternative trajectories of simulations using a constricting and simultaneously elongating cuff potential. For each trajectory, a snapshot indicating the location of initial nucleation of the micelle topology (top) and another snapshot indicating the rupture of the wormlike micelle (bottom) are shown. The duration of the ongoing topological change between the two snapshots varies (A: 540τ , B: 290τ , C: 140τ), but the locations of nucleation for micelle formation and rupture is remarkably close. The patterned bar shown in the lower left of A corresponds to a distance of 2σ .

Table 1 Time t and cylinder radius R_{cuff} at which the wormlike-micelle topology first is observed (WLM, corresponding to the state shown in Figs. 6 C, 7 C and 8 C), and at which the connection between the two sides is finally severed (RUP, corresponding to the state shown in Figs. 6 F, 7 F and 8 F). The headings indicate the length l_{cyl} of the cylindrical cuff, the tension Σ_x in the x direction, or that an elongating cuff potential was used.

$l_{\text{cyl}} = 2 \sigma, \Sigma_x = 0 k_B T \sigma^{-2}$						
	$t [\tau]$	$R_{\text{cuff}} [\sigma]$				
WLM	6770	5.08				
RUP	8360	3.49				
$l_{\text{cyl}} = 6 \sigma, \Sigma_x = 0 k_B T \sigma^{-2}$						
	$t [\tau]$	$R_{\text{cuff}} [\sigma]$	$t [\tau]$	$R_{\text{cuff}} [\sigma]$	$t [\tau]$	$R_{\text{cuff}} [\sigma]$
WLM	6630	5.22	6640	5.21	6580	5.27
RUP	8230	3.65	7990	3.86	7520	4.33
extending cylinder, $\Sigma_x = 0 k_B T \sigma^{-2}$						
	$t [\tau]$	$R_{\text{cuff}} [\sigma]$	$t [\tau]$	$R_{\text{cuff}} [\sigma]$	$t [\tau]$	$R_{\text{cuff}} [\sigma]$
WLM	6650	5.20	6750	5.10	6820	5.03
RUP	7190	4.66	7040	4.81	6960	4.89
$l_{\text{cyl}} = 6 \sigma, \Sigma_x = 0.01 k_B T \sigma^{-2}$						
	$t [\tau]$	$R_{\text{cuff}} [\sigma]$				
WLM	6680	5.17				
RUP	6860	4.99				

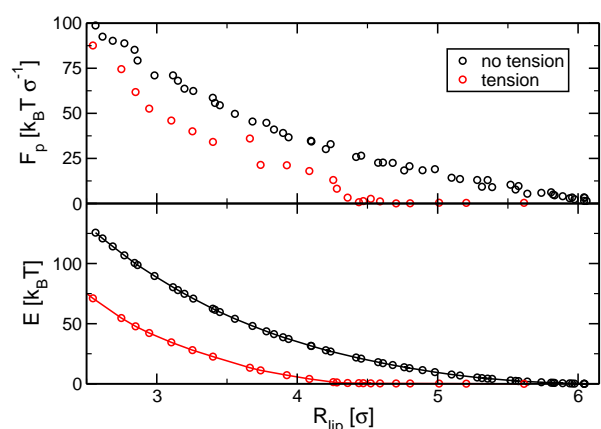


Fig. 10 Plot of the force F_p the cuff potential exerts in a direction perpendicular to the cylindrical bilayer in dependence on the bilayer's radius R_{lip} , and the free energy E of the created constriction. The length l_c of the cylindrical mantle around which the cuff potential is defined was 2σ . Shown are data for a tensionless lipid tube, and a tube for which a tension of $0.01 k_B T \sigma^{-2}$ was applied in the x direction.

on the other hand, also indicates how many lipids are affected in total. Fig. 11 shows that the majority of the free-energy cost arises at the periphery, especially for narrow cuff radii, whereas the lipids within the cylinder do not only experience less force individually, but also are less in numbers. The latter observation stems from the fact that the lipid bilayer wraps

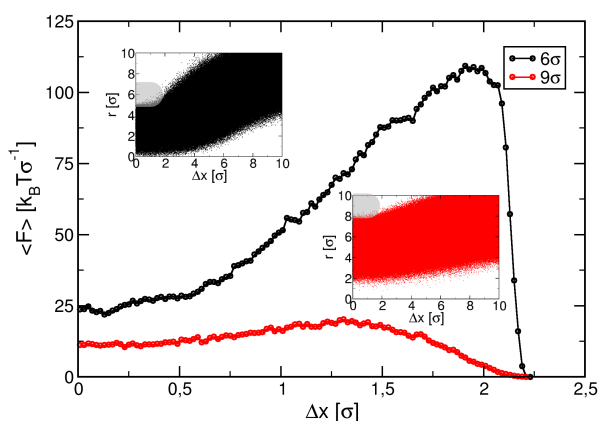


Fig. 11 Average force, $\langle F \rangle$, that the cuff potential exerts on the cylindrical lipid bilayer in dependence on the position along the cylinder axis, defined by the distance, Δx , from the cuff's center. The length l_c of the cylindrical mantle, around which the cuff potential is defined, is 2σ , and the cuff's radius was set to the values given in the key. Note that the cuff's mantle ends at $\Delta x = 1\sigma$. The insets present projections of the lipid coordinates into the x - r plane with the region subject to the potential highlighted as gray shaded area.

around the constricting potential as illustrated in the insets in Fig. 11, which leads to a larger portion of bilayer area being projected onto a length unit on the x -axis.

We also were able to study the changes in particle density caused by the constriction. Fig. 12 shows a representative plot for a system with a cylinder radius of 8σ and a cylinder length of 2σ . There is a pronounced increase in head-group density in response to the constriction, reflecting the increased curvature and decreased area available to the lipids in that region. The density profiles were obtained after an equilibration time of 2500τ . The lipids therefore had ample time to redistribute within their respective monolayers, but not between the monolayers, which is realistic on the time scale of fission.

3.2 Dynamins as rings of amphiphilic discs

In order to investigate the role of the shallow insertion of the PH domains of the dynamin complex into the lipid bilayer, we replace the structure-less cuff-potential by a representation for peptides in our coarse-grained membrane model. These peptides use the same particle types as the lipids, i.e. head-group and tail particles, and we impose the desired structure using a network of harmonic bonds, as described in Sec. 2. Rather than using a helical arrangement of the PH domains, we used a circular arrangement, which, apart from being easier to setup, may well correspond to the smaller dynamin complexes as-

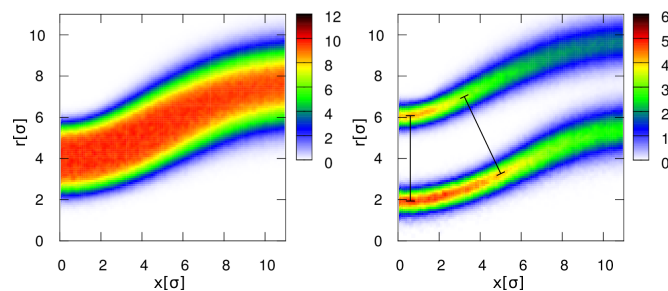


Fig. 12 Particle densities in units of σ^{-3} for tail (left) and head-group beads (right). The cuff potential used a cylinder radius of 8σ and a cylinder length of 2σ located at $x = 0$. The two markers used to measure the bilayer thickness in the plot of the head-group density have the same length.

sembling in the presence of GTP. In this setup, 12 of our amphiphilic disks were restrained to positions evenly spaced on a ring of a specified radius on the cylindrical membrane tube, with only the center-of-mass' location affected, whereas the orientation of the disks was completely free to react to its surrounding.

3.2.1 One ring– First we consider a single, 12-peptide ring around a membrane tube. By gradually decreasing the ring radius between the simulations, we constrict the membrane tube within a series of constant radius simulations. Fig. 13A shows the average radius of the cylindrical lipid bilayer as a function of the x -coordinate. For all radii, we find that the peptides' position is *not* the most narrow part of the tube, i.e. there is actually a positive curvature component at the peptides' location.

To test whether a symmetric or asymmetric membrane shape better accommodates this curvature requirement, we mirrored each snapshot of the trajectories so that the minimal radius was always at a positive x -coordinate prior to averaging (see Fig. 13A). While this treatment creates a bias, it provides some information on the shape of the constricted system, which would be lost with ordinary averaging that would inevitably lead to a symmetric shape because the position of the minimum occurs with equal probability on either side of the peptide ring. At intermediate constriction the profile is asymmetric, whereas, at smaller constriction radii, the system becomes more symmetric and the minima move closer to the peptides' position. Fig. 13 A clearly indicates an abundance of asymmetrically shaped snapshots but it is difficult to make quantitative statements. Even in the absence of a peptide ring, there will be some asymmetry because one of the two minimal values of the radii in the two halves of the tube will be smaller than the other.

Therefore, we studied the distribution, $P(x)$, of the minimum's location. Fig. 13 B plots a histogram of the x -

coordinate along the tube axis at which the minimal tube radius is observed for a selection of peptide ring radii. In agreement to our discussion of Fig. 13 A, a symmetric, bimodal distribution with the most likely minimum locations lying on either side of the peptide ring is observed. In addition, the distribution is relatively wide for low constriction, and becomes narrower with increasing constriction. The separation between the two peaks decreases with increasing constriction, but a fit to a double Gaussian distribution of the form

$$P(x) \sim \exp\left(-\frac{(x-x_0)^2}{2d_{x_0}^2}\right) + \exp\left(-\frac{(x+x_0)^2}{2d_{x_0}^2}\right) \quad (2)$$

reveals that the distribution remains bimodal even at the strongest constriction investigated.

While these single-ring simulations illustrate the pronounced deformation of the membrane tube, even at the smallest ring radius of 5.5σ and a simulation time of 1200τ , no topological change to a wormlike micelle structure or fission was observed.

3.2.2 Two rings— In the next set of simulations, we tested whether neighboring rings might cause a constructive overlapping of deformation effects in their middle. We used a similar setup as above with two rings at a distance of 6 to 12σ . Again each ring is comprised of 12 peptides. However, rather than starting at the equilibrium radius of the cylindrical bilayer, we used a stretched and therefore much narrower conformation that we had obtained by applying tension along the cylinder axis. With this setup, we were able to place the peptide disks at the desired position with ring radii as small as 5.0σ without penetrating deeper than their spontaneous position into the lipid bilayer. By setting the tension back to zero in the production runs, the system re-expanded its radius subject to the imposed constriction. The expansion occurred on a time scale faster than lipid flip-flops and topological changes (less than 50τ versus 40000τ and 300τ , respectively), thus, we consider the setup suitable for studying deformation and fission.

Fig. 14 shows the average radius of the cylindrical bilayer as a function of the position, x , along the cylinder axis in the presence of the two peptide rings for a selection of ring radii r and distances d between the rings. Interestingly, we find that the two parameters have a pronounced influence on the observed deformation, but the direction of the effect critically depends on their combination. At the larger ring radius of 8σ , we find that there is a pronounced minimum in-between the rings at ring separations of 10 and 12σ , whereas at a separation of 6σ , the minima actually lie outside of the region enclosed by the peptide rings. At the smaller ring radius of 5σ , on the other hand, the trend is reversed, and we find the most pronounced minimum between the rings at the closest ring distance of 6σ . At larger ring separations, we find a less constructive interference of the rings' effects, and observe two

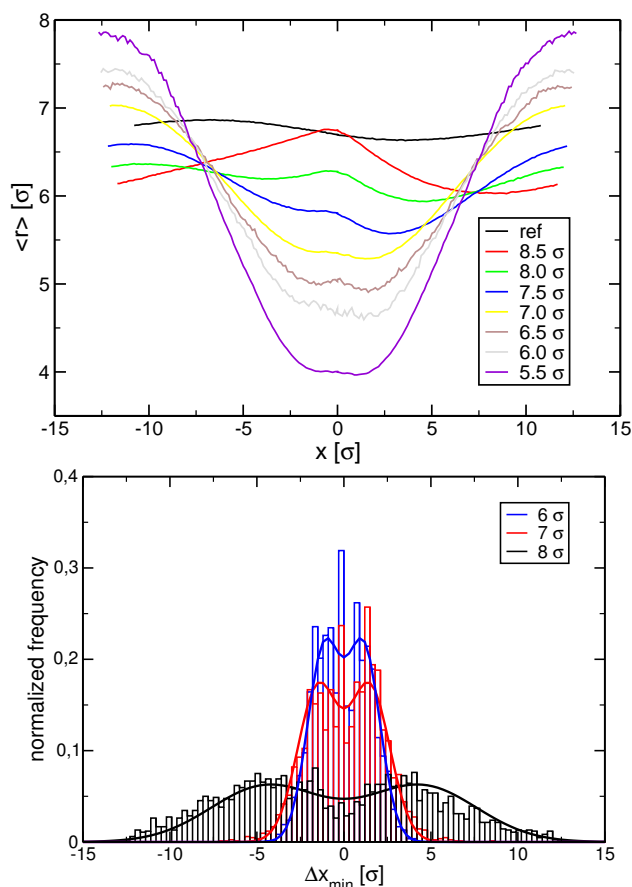


Fig. 13 (top) Average radii r of membrane tubes (center to bilayer's midplane) around the x axis, including a ring of 12 dynamin peptides (with a radius specified in the key) at $x = 0\sigma$. The individual frames of the trajectory were always turned so that the minimal radius was at the right side of the peptides prior to averaging. As reference, a membrane tube without peptides is also included. (bottom) Histogram of the distance Δx_{\min} from the peptide ring at which the minimal tube radius is observed for a selection of peptide ring radii. In addition, fits to the double Gaussian distribution, Eq. 2, are also shown.

separate minima within the region enclosed by the rings at a separation of 12σ , and a single minimum at a separation of 10σ . In the latter case, however, the constriction is less pronounced than the constriction at a separation of 6σ . In addition, we again consistently find a positive curvature at the location of the peptide rings, which is clearly visible as “bends” in the profiles shown in Fig. 14.

However, even this arrangement of dynamin rings did not induce a lasting topological change within the duration of our simulations, 7500τ . However, in the system combining a ring radius of 5σ and a separation of 6σ , which displayed the largest constriction of the simulated systems (cf. Fig. 14), we

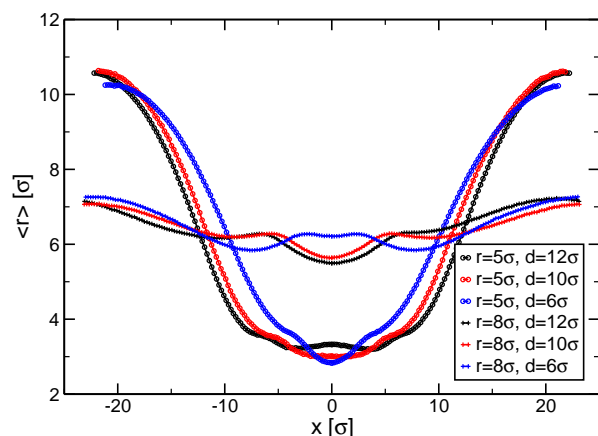


Fig. 14 Average radii r of membrane tubes (center to bilayer's midplane) around the x axis, including two rings of 12 dynamin peptides restrained to a ring of radius r and a separation d specified in the legend. The peptide rings are restrained to $x = \pm d/2$.

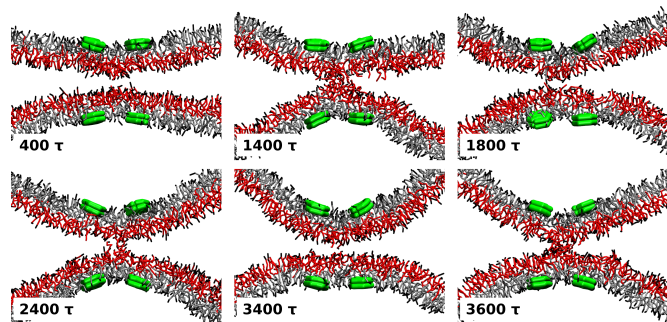


Fig. 15 Cross-section through the midplane of a lipid bilayer tube constricted by two peptide rings of 5σ radius and a separation of 6σ . Lipids originating from the outer and inner monolayer are rendered in gray and red, respectively, with black color marking the head-groups. The peptide disks are shown in green. The lumen of the membrane tube repeatedly opens and closes during the course of the simulation.

observed temporal closure of the bilayer tube's lumen, resulting in a stable flickering state shown in Fig. 15.

We also conducted simulations studying the effects of tension on the constriction. To this end, we used the system for which we observed the smallest radius, i.e. a ring radius of 5σ and a ring separation of 6σ . As shown in Fig. 16, applying a tension of $0.01 k_B T \sigma^{-2}$ in the direction of the cylinder axis reduces the amount of constriction. However, when applying a negative tension of $-0.01 k_B T \sigma^{-2}$, effectively compressing the system along the cylinder axis, the amount of constriction increased and the constricted region assumed a wormlike micelle topology within 500τ . This topology then persisted without further change for the remaining 6500τ duration of the simulation.

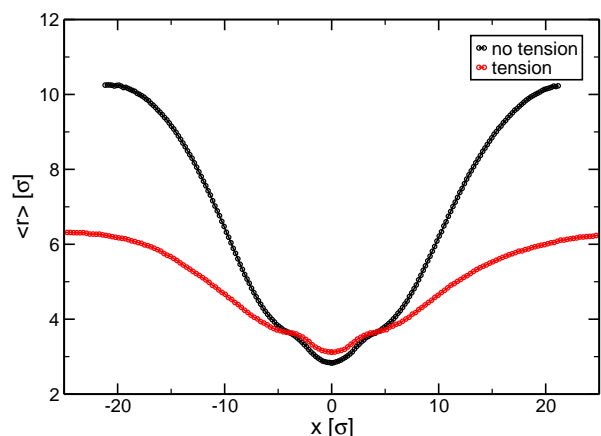


Fig. 16 Average radii r of membrane tubes (center to bilayer's midplane) around the x axis, including two rings of 12 dynamin peptides restrained to a ring radius of 5σ and positions $x = \pm 3\sigma$. Shown are plots of a tension-free system (no tension), and a system with a tension of $0.01 k_B T \sigma^{-2}$ applied in the direction of the cylinder axis (tension). A third system with negative tension of $-0.01 k_B T \sigma^{-2}$ displayed an increased constriction and undergoes topological changes within 500τ (data not shown).

Using the peptides' average displacement from their anchor points, we measured the force, F_p , that the peptides exert on the lipids in the radial direction perpendicular to the cylinder axis. Fig. 17 plots these radial forces for the two-ring systems as well as for the one-ring system reported in the previous section. As expected, F_p becomes larger the smaller the ring radius is. In addition, for the two-ring systems, the force also increases the wider the separation between the rings is. Thus the force appears to be more sensitive to the width of the constricted region than its maximal constriction, which is the largest for the smallest separation (cf. Fig. 14). Compared to the force exerted by the cuff potential (cf. Fig. 10), the total radial force needed to keep a certain amount of constriction is comparable in magnitude but slightly smaller. Specifically, we observe the values of 38.32 and $36.48 k_B T \sigma^{-2}$ for the cuff and single-ring system, respectively, with a similar maximal constriction but a significantly longer constricted region for the single-ring system using peptides (see Fig. 23 / Electronic Supplementary Information (ESI)).

3.2.3 Two double-rings– In order to explore if additional curvature can overcome the threshold for topological changes, we replaced the two peptide rings with two double-rings, each consisting of two rings at a small separation d_{intra} . We still used 12 peptide disks per ring, but by assigning different radii to the two subunits of the double-rings, we exert more influence on the bilayer's orientation at the location of the peptide complexes and can emulate the intrinsically hourglass-shaped geometry of the neck of an invaginated pit. Otherwise, the

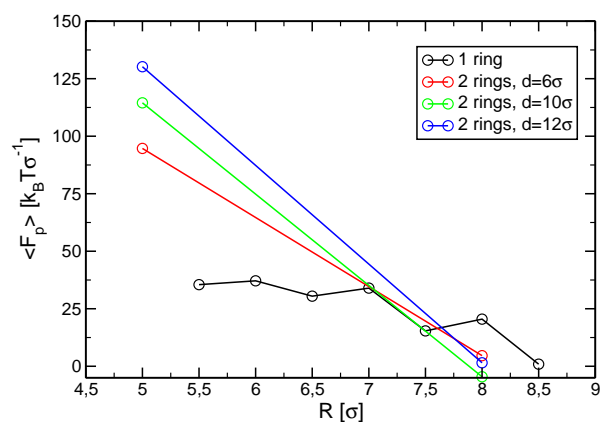


Fig. 17 Plot of the total average force $\langle F_p \rangle$ the amphiphilic disks exert on the lipid bilayer tube in dependence on the ring radius R and the rings' separation d . Results are shown for systems containing one as well as two rings.

setup was the same as for the simulations using two single rings described in the previous section.

Table 2 gives an overview of the performed simulations and their outcomes. By assigning larger radii to the outer subunits of the double-rings, we actively create a default “slope” in the orientation of the bilayer at the location of the double-rings in addition to the curvature created by the insertion of the amphiphilic disks. In some simulations, this setup led to the closure of the cylinder lumen and the formation of a stalk or wormlike micelle region between the double-rings by “fusion” of the inner monolayer and subsequent leaving of the lipids of the inner monolayer from this area until only lipids from the outer monolayer were left in the stalk. Whether topological changes occurred depended on the amount of constriction and the separation of the double-rings, but the outcome was most sensitive to the amount by which the radius of the outer rings had been increased with respect to the inner rings. As an example, at a separation d_{inter} of 6σ and a radius R of the inner rings of 5.5σ , only one out of three simulations underwent topological changes with a radial difference ΔR of 0.5σ , while all simulations changed for radial differences of 0.75 and 1.0σ even when using larger inner ring radii of 5.75 and 6σ , respectively.

Fig. 18 shows the average radius in dependence of the position along the cylinder axis for a system containing two double-rings separated by a distance of 6σ and a ring radius of 5.5σ , with the outer units shifted by a distance of 0.5σ away from the center in the x -direction, and also by 0.5σ in the radial direction. Compared to a system containing only single-rings at an even smaller radius of 5σ , we find a significant reduction of the radius in between the two double-rings that was sufficient to trigger a topological change in one out of the three simulations conducted with this set of parameters.

Table 2 Results of simulations in which curvature was controlled by representing dynamins as double-rings. In these simulations, each dynamin ring was duplicated by inserting a second copy at a slight offset, d_{intra} , along the cylinder axis. By assigning an increased ring radius to the outer copies, indicated by the radial difference ΔR , we were able to introduce variable curvature into the system. The ring radius for the inner copies is R , and their distance along the axis is d_{inter} . Depending on the system, we find curved, hourglass-shaped constrictions (cc), in which the dynamin complexes reside within the curved part of the constriction, or flat constrictions (fc), in which hourglass-like curvature is mainly localized outside of the dynamin complexes. In addition, in some cases, we observe the formation of a stalk-like topology between the two dynamin double-rings (st). Numbers in parentheses indicate the number of simulations, in which the indicated result was observed for parameter combinations for which multiple simulations were performed.

R [σ]	d_{inter} [σ]	d_{intra} [σ]	ΔR [σ]	result
5	10	0.5	0.5	cc
5	10	0.5	1.0	st
5	10	0.5	1.5	st
5	10	0.5	2.0	st
5	10	2.5	2.5	st
5	6	0.5	0.5	st
5	6	0.5	0.0	fc(3)
5	6	1.0	0.0	fc
5	6	2.5	2.5	st
5	6	0.5	0.5	st(3)
5.5	6	0.5	0.5	cc(2),st(1)
5.5	6	0.5	0.75	st
5.5	6	0.5	1.0	st
5.5	6	0.5	1.5	st
5.5	6	0.5	2.0	st
5.75	6	0.5	0.75	st(3)
6	6	0.5	1.0	st(3)
6	10	0.5	0.5	cc
6	6	0.5	0.5	cc

In addition, simulations using double-rings in which the inner rings were held at the smaller radius of 5σ and the outer units were restrained to the same radius so that there was no difference in radius between the subunits, showed even less reduction of the radius in between the two double-rings than the single-ring system, and exhibited no increased tendency towards persistent topological changes. However, in these systems, in which the double-rings' subunits had the same radius, we observed transient closure of the cylinder's lumen (flickering) as described above for the single-ring system. This flickering was observed both in the region between the two double-rings and on the outside, as visible in Fig. 19 A.

However, even when continuing the simulations in which a stalk-like topology had formed for 6000τ , we did not ob-

serve the completion of the fission process by rupture of the stalk. Even when removing the peptides from the configuration by simple deletion of the corresponding particles in the simulation, the stalks remained stable during the 4500 τ continuation of the simulation. The same is true for simulations in which only the restraints on the peptide positions but not the peptides themselves were removed after the wormlike micelle stage was reached.

To determine the effects of tension on the transition from wormlike micelle to the completion of fission, we used systems with 6 and 10 σ separation between the double-rings. The exact system parameters of the two sample systems, named A and B for easier reference, are listed in Table 3. When applying a tension of $0.01 k_B T \sigma^{-2}$ along the cylinder axis, the systems remained stable for the duration of 9000 τ simulations, when the peptides remained fixed at their assigned positions. Only when the restraints on the peptides' positions were lifted, allowing the peptides to freely diffuse, did the connection break and the fission complete after 2400 τ for the system with the 6 σ ring separation, whereas the system with a 10 σ ring-separation remained stable also at this tension. In order to test the apparent stabilization of the wormlike micelle by the restrained peptide complex, we increased the tension to $0.1 k_B T \sigma^{-2}$. Even at this level of stress, the systems with restrained peptides remained stable for 3200 τ simulations, whereas in simulations with lifted restraints on the peptides, the wormlike micellar region ruptured within 100 τ .

Table 3 System parameters for the sample systems subjected to tension in an attempt to reach completion of fission.

System	R [σ]	d_{inter} [σ]	d_{intra} [σ]	ΔR [σ]
A	5.75	6	0.5	0.75
B	5	10	0.5	1.0

4 Discussion

4.1 Deformation

One of the basic pre-requisites for fission is the creation of a constriction, in which the lumen becomes narrow enough for the inner monolayer to form a diaphragm, sealing the channel through the constriction. Before considering this topological change itself, it is therefore interesting to study the deformation leading up to this first topological transition.

Our simulations of constriction of a cylindrical membrane topology correspond to experimental setups in which lipid nanotubes are constricted and cleft in the presence of dynamin^{15,17,22,24,40}. In this setup, there are no morphological boundary conditions that imply a neck-like constriction

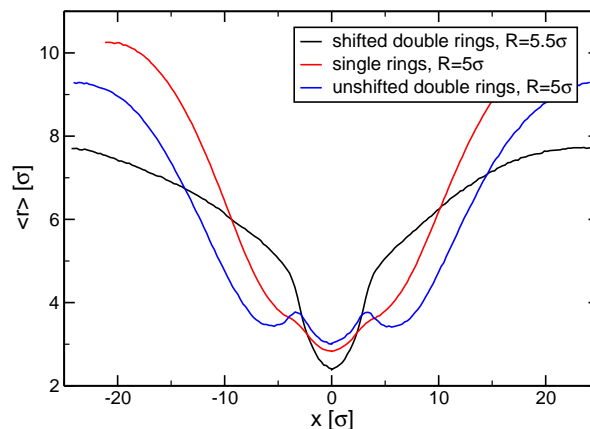


Fig. 18 Average radii r (center to bilayer's midplane) of a membrane tube around the x axis, including two double-rings, with the inner units restrained to a ring radius of 5.5σ and a separation of 6σ and the positions of the outer units shifted away from the center by a distance of 0.5σ in the x direction and also by 0.5σ in the radial direction (shifted double-rings). In comparison, a system containing single rings at a (smaller!) radius of 5σ at the same separation of 6σ (single rings), and a system containing double-rings, where the inner units are restrained to positions identical to the single ring system, and the outer units are shifted only along the x -axis, but not in the radial direction (unshifted double-rings) are also shown. The inner peptide rings are restrained to $x = \pm 3 \sigma$.

smaller than the cylinder diameter, which contrasts with the hourglass-shaped neck of an invaginated clathrin coated pit, in which a reduction of the neck diameter may actually represent an option to reduce the curvature stress of the fusion pore-like topology.

We find a free-energy cost of approximately $125 k_B T$ to locally reduce the cylinder radius from its equilibrium value of 6 to 2.5σ in a tension-free lipid tube. While this value agrees nicely with previous findings based on elastic models^{2,3}, it appears to be a rather high barrier to be overcome by the dynamin complex alone, which only has a polymerization energy of $3.8 k_B T$ per dimer⁴⁰, suggesting the involvement of additional factors. We expect that one such factor is membrane tension, which is usually present in experimentally produced lipid tubules and by itself can reduce the tube diameter up to the point of rupture. In our simulations, we were able to reproduce this property and find a reduced free-energy cost of about $75 k_B T$ to achieve a similar constriction as above in a system with a tension of $0.01 k_B T \sigma^{-2}$ along the tube axis (x direction). However, it should be pointed out that this reduction is predominantly due to a thinner starting radius under tension and does not stem from a reduced cost of creating the curved geometry of the constriction.

Another important factor is induction of local curvature due

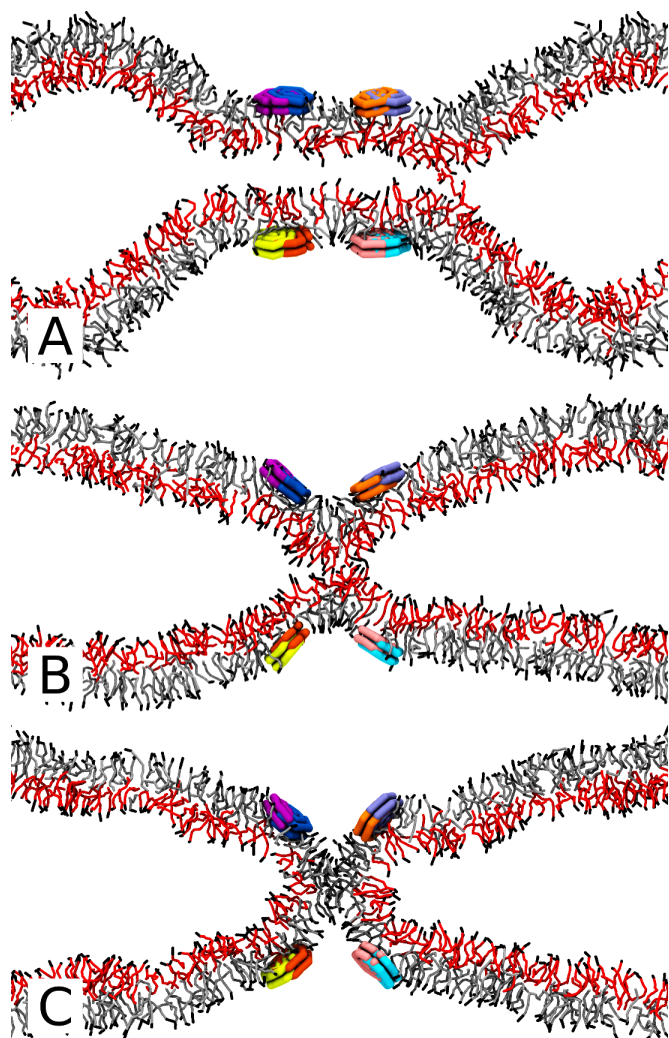


Fig. 19 Snapshots showing cross-sections through the midplane of the final configurations of the systems described in Table 2. (A) If the two subunits of the double-rings have identical radii, no (positive mean) curvature is created at the peptides' position, and the constricted area is cylindrical with additional curvature limited to the regions outside the peptides. (B) When the radii of the inner subunits are smaller, the double-rings participate more directly in the creation of curvature and the location of the saddle-splay curvature of the created hourglass-shape coincides with the peptides' position. (C) If enough curvature is induced, the lumen of the cylindrical bilayer closes between the two double-rings and a wormlike micellar or stalk-like topology is created. The head-groups visible in the center of the wormlike micelle are an misleading artifact of the visualization and actually lie before or behind the center. The systems shown have the same parameters $R = 5\sigma$, $d_{\text{inter}} = 6\sigma$ and $d_{\text{intra}} = 0.5\sigma$, with only ΔR differing within a range from 0σ (A) to 0.5σ (B, C).

to the shallow insertion of peptides, which we investigated by

representing the membrane interacting PH domains by a circular arrangement of amphiphilic disks. These peptide rings around the lipid tubes not only constrict the system by imposing a certain radius at their position, but they locally change the particle density in the outer monolayer as shown in Fig. 4. The so-created asymmetry between the monolayers gives rise to a positive spontaneous curvature, which we were able to demonstrate both for a single ring of peptides (Fig. 13) and systems including two rings at various separations (Fig. 14). This local positive curvature conflicts with the global requirement of a negative curvature of the constriction. This frustration is resolved by increasing the constriction next to the point of insertion even further than the value imposed by the ring radius in order to locally create the positive curvature induced by the PH domain insertion. For systems with only a single peptide ring, this additional constriction can occur at either side of the ring with equal probability, as shown in Fig. 13 B. For systems with two rings, however, we found a pronounced interplay between the shape requirements of the two rings, which creates a constructive interference of the constriction between the rings for favorable parameters. In our simulations, this effect depends both, on the ring radius and the separation. For a ring radius only a little smaller than the bilayer tube, the constructive interference is especially pronounced for the largest ring separation of 12σ whereas, at the smallest ring separation of 6σ , the additional curvature was actually created outside of the region between the two rings. This observation can be rationalized when one considers the preferred distance d_{min} of the maximal constriction to the ring position. Fig. 13 B shows that this distance decreases with increasing constriction, implying that for the constructive addition to be most effective, the ring separation should correspond to roughly twice d_{min} . If the ring separation is smaller, the position of the respective minima induced by the one ring moves towards the other, discouraging the additional constriction because the membrane in the immediate neighborhood of the peptide rings has to match the peptides' positions because of attractive interactions with the amphiphilic disks. For the same reasons, the smallest used ring separation of 6σ creates the most pronounced additional constriction for small ring radii and large constriction.

Within the experimental dynamin complex, however, the separation between the helical turns is not variable but imposed by the dynamin proteins and has been reported to be approximately 10nm^{41} . While this value changes as a consequence of conformational movement of the dynamin complex, we cannot expect it to vary within the range used in our simulations. While the detailed effects of shallow peptide insertions depend on factors that our coarse-grained representation of the PH domains of dynamin may not quantitatively represent, we expect our model to capture the qualitative trend.

In addition, certain factors can have very complex effects on the system, an example being bilayer tension. While naively

one would expect the constriction to increase when applying tension along the cylinder axis, we found this not to be the case with the additional constriction induced by insertion of amphiphilic disks, and the minimal radius actually increased under tension (Fig. 16), whereas a negative tension increased the constriction and even triggered topological changes which were not observed in the tensionless system. This behavior can be understood when taking into consideration that the bilayer radius at the positions of the peptide rings is restricted to the ring radius due to the attractive interactions with the peptides, and will not reduce in response to moderate tension. With these boundaries, having a curved, hourglass-shaped constriction between the two rings becomes unfavorable, as the increase in area relative to a flat, cylindrical shape is penalized by the tension.

The local creation of additional positive mean curvature needs to be addressed in more detail. In our simulations, it is created by shallow insertion of an amphiphilic peptide disk, which is in line with experimental observations of a significant insertion of the PH domain²⁷. However, the origin of the curvature needs to be distinguished from its effects, which can be considered to be largely independent from the manner in which the change in spontaneous curvature has been created, and a more specific mode of curvature creation, relying on dynamin's lipid binding pocket^{24,28}, can be expected to have a similar influence on the fission pathway.

Reports that the membrane association of the PH domains of dynamin does not induce curvature⁴², on the other hand, do not agree with our simulation results, but may originate from the experimental setup using isolated PH domains, which does not allow the polymerization that is mediated via other parts of the dynamin proteins. Apart from the constriction associated with the formation of a helical protein complex, polymerization also coordinates the relative locations of the PH domains and results in a high concentration of PH domains along the "path" of the polymeric complex, which is lost in the experimental setup used in ref.⁴². It is hard to envision how such a highly anisotropic arrangement of membrane insertions would not influence the local spontaneous curvature along the created belt, even if the individual insertions were shallow and of only moderate density as in our simulations. Our simulation findings clearly indicate such a curvature inducing effect. However, this effect may not be sufficient to induce fission from a planar template, and it is possible that it requires a pre-curved morphology to achieve fission.

These effects, i.e. the role of the membrane geometry, which for the necks of invaginating pits or budding vesicles is more similar to that of a large fusion pore than to that of a cylindrical membrane tube, we took into consideration with a different set of simulations: In these simulations we replaced the single-rings of amphiphilic disks by double-rings, in which we gave each ring an additional partner-ring shifted

a small distance of 0.5σ along the cylinder axis. By assigning a larger radius to the outer ring, we could effectively define a default slope of the bilayer at the position of the peptide insertion. With this setup, we observed a dramatic increase in constriction as shown in Fig. 18, and we were able to trigger topological changes at ring radii at which no changes occurred for single-rings. While these effects may be partially due to the additional curvature imposed by doubling the peptide particles in the system, we consider the main factor to be the combination of a predefined slope together with additional positive curvature. This is demonstrated by the fact that the use of double-rings with identical radii for both units did not enhance the constriction, but actually reduced it.

The additional constriction due to the positive curvature introduced by the shallow insertion also has implications for the minimum radius that a constricting protein complex needs to reach in order to generate a certain amount of constriction. With shallow insertion, we find the radius of the constriction to be up to 1σ less than the bilayer radius at the site of interaction with the peptides (cf. Figs. 14 and 13), whereas isolated constrictions, generated by a cuff potential, created a minimum at the site of interaction. This implies that the distance, by which an element – be it repulsive potential or amphiphilic disk – needs to be forced against the bilayer to reach a certain level of constriction can be reduced by the additional creation of local curvature. In addition, our simulations using intrinsically sloped bilayers with the help of double-rings suggest that the amount by which the maximum constriction exceeds the constriction at the site of the interactions with the peptides can be drastically increased within the intrinsically hourglass-shaped geometry of the fusion-pore-like environment of the neck of an invaginated pit or budding vesicle (cf. Fig. 18).

The latter finding is interesting in the context of reports that some dynamin variants are unable to induce fission in the absence of a preformed invaginated pit⁴³. While this data has been linked to the requirement of limiting fission to specific sites in non-neuronal cells⁴³, it also shows that dynamin variants with a weakened ability to induce fission can do so in a preformed hourglass-shaped geometry as in our simulations using double-rings, while they are unable to do so otherwise.

Concerning the steep free-energy increase upon constricting the membrane tube by the cuff potential, however, the shallow insertion of the PH domains does not appear to result in a drastic reduction. While we do not have the data to allow a direct calculation of the free energy for these simulations, the measured perpendicular force of $94.68 k_B T \sigma^{-1}$ for the two-ring system with ring radius 5σ and a ring separation of 6σ (cf. Fig. 17), in which we observed first topological changes in the form of flickering, suggests that still a significant energy barrier is needed to reach sufficient deformation when starting from a cylindrical geometry.

4.2 Topological changes

After a sufficient level of constriction has been reached, the actual topological changes occur. In our simulations using a constricting potential without insertion of peptides, the lipid tube had to be “squeezed” all the way until its lumen only consisted of lipid head-groups, when at some point the connectivity of the head-groups in the inner monolayer broke and the seed of a wormlike micelle formed. We did not detect a clear preference of location for this seed to form, and when using longer cuff potentials, it formed somewhere within the constricted area, but at least a lipid length away from its edge. Using the rupture of the inner monolayer, i.e. the local wormlike micelle formation, and the rupture of the outer monolayer, i.e. the final rupture of the connection, as the most clearly defined markers of the fission process, we found that when there was no tension in the system, the wormlike micelle stage was stable on the μs scale accessible to our simulations when we did not further decrease the radius of the cuff potential, indicating that if constriction is the only mechanism by which a peptide induces fission, it has to drive the process almost all the way and actively cleave the constricted lipid bilayer.

If the system was under tension, either by explicitly applying tension or using a cuff potential that simultaneously constricted and extended its length, the wormlike micelle stage occurred at the same level of constriction as in the tensionless system, but once this stage was reached, the transition to the final rupture of the connection proceeded within a few hundred ns, indicating that under these conditions, wormlike micelle formation is the transition state that faces a significant free-energy barrier, whereas the rupture of the wormlike micelle is a spontaneous event (cf. Table 1). In this aspect, our data therefore supports the hypothesis that the elongation caused by the conformational change of the dynamin complex after hydrolysis of GTP plays an important role in fission^{17–19}. However, it is unclear whether the dynamin complex can create extensive movement of its domains with sufficient speed to cause tension or shearing stress, and experimental evidence indicates that the movement of the dynamin complex is not continuous but periodic, and occurs on a timescale significantly slower than lipid diffusion and shape relaxation²².

In addition, the observed necessity to constrict the bilayer tube all the way up to the point at which the inner walls touch or even push against each other, disagrees with the experimental finding that a spontaneous topological change, resulting into a closure of the lumen, already occurs when the lumen's diameter is reduced to approximately the value of a bilayer thickness^{20,44,45}, and makes a purely constriction-based mechanism of fission unlikely.

If we constrict the system using rings of amphiphilic disks that shallowly insert into the lipid bilayer, it is no longer the constriction alone that pushes the inner monolayer inwards but

rather the additional curvature causing an even greater constriction at a certain distance away from the location of the peptide ring, especially if there are two peptide rings at a separation suitable for constructive overlap of this additional constriction.

A first difference to the results using a cuff potential is therefore the observation of a flickering state, at which a transient diaphragm closing the lumen repeatedly forms and disappears in the constricted region between the peptide rings (cf. Fig. 15). Such a state, in which an open and a closed state interchange on a timescale faster than protein assembly and disassembly, is also observed in experimental conductance measurements through lipid tubules constricted by dynamin²⁴. It is hard to envision in regions where fluctuations of membrane shape are suppressed, as in bilayer areas that are in direct contact with parts of a rigid protein complex, regardless whether the interactions are attractive or repulsive, because in the latter case the membrane's rigidity will usually push the membrane against the boundary. However, if the constriction is generated in an indirect, softer way, like via local creation of curvature and occurs at a distance from the insertion, there are sufficient fluctuations to allow the flickering between a closed and an open state of the constricted region.

It is interesting to note that if the peptide ring radius does not change, this flickering state appears to persist without going in either direction along the path from membrane tube to fission because the fixed bilayer radius (directly at the peptide ring) keeps the lumen from permanently collapsing. In this sense, a stable protein complex around a cylindrical bilayer can actually stabilize the cylinder even while causing a large amount of constriction and inducing additional curvature, which is in accord with experimental observations in which dynamin coated bilayer tubules are stable at smaller radii than uncoated tubules²³ and similar findings that were reported for BAR domain proteins³⁶.

When using double-rings to emulate an intrinsically hourglass-shaped environment, we were able to induce the formation of a wormlike micelle or stalk connection in the constricted region without further reduction of the ring radius. Interestingly, again this stage will be stable if the peptides are kept at the positions, at which they had triggered the topological change. Even when applying significant levels of tension, we cannot induce rupture of the connection within the μs scale of our simulations. Only when we released the constraints on the peptides' centers of mass and allowed them to freely diffuse on the tube or removed the peptides completely, did fission proceed further by rupture of the wormlike micelle. It is therefore possible that if a complex of fission proteins triggers the initial stage of fission by forming a stable, constricting mold with strategically placed shallow insertions, it will stabilize the wormlike micelle stage to a degree that it will not break under thermal fluctuations or even constitutes a stable

state, and it is necessary for the protein complex to disassemble before fission can be completed. This scenario agrees with experimental observations that require the dynamin complex to fall apart before fission occurs²² as well as studies that show a stabilizing effect and stable cylindrical micelles in the presence of BAR domain proteins^{36,46}.

5 Conclusions

Our data suggests that a fission mechanism relying exclusively on constriction does not constitute a feasible option for dynamin-mediated fission. In the absence of other factors, constriction would need to drive the fission process all the way from first deformation until rupture of the wormlike micelle, which requires formation of an extremely narrow protein complex and an energetic cost that exceeds the free energy available from polymerization of dynamin⁴⁰.

Under the assumption that the PH domains of dynamin cause a shift of the spontaneous mean curvature to more positive values, the necessity to form a narrow protein complex becomes alleviated, because the need to fulfill the curvature requirement causes an additional constriction at a small distance from the point of membrane contact that exceeds the constriction at the peptides' location. Such an effect on curvature could originate from shallow insertion of peptide moieties into the lipid bilayer as in our simulations, or from more specific lipid-peptide interactions like a binding pocket pulling lipids out of the bulk reported in refs.^{24,28}. If more than one strand of the constricting protein complex are taken into account, we showed that constructive overlap of the additional constriction of neighboring strands has a cooperative effect that further reduces the necessity to mechanically "squeeze" the bilayer tube.

Another consequence of the more indirect way of generating constriction via curvature frustration is that, since maximal constriction occurs at a distance from the peptides, shape fluctuations are possible that would be suppressed in a region in direct contact with a rigid, bulky protein complex. These fluctuations can be expected to be important for forming the seed of topological transformations, and also manifest themselves as a flickering state, in which the cylindrical bilayer lumen repeatedly opens and closes in our simulations. Without disassembly of the protein complex, this flickering state appears to be stable, and its existence is supported by experimental conductance measurements²⁴.

By artificially imposing an hourglass-shaped geometry in the surroundings of the constriction, we were able to facilitate formation of a wormlike micelle configuration. Just as the flickering state, this configuration was stable for the duration of our simulations when the conditions that led to its formation persisted, i.e. the protein arrangement was not disassembled and even survived application of significant tension. This

observation agrees with experiments using BAR domain proteins⁴⁶.

We therefore conclude that the dynamin complex and similar protein complexes involved in fission can help to trigger topological changes by stabilizing the wormlike micellar transition state, but need to undergo disassembly for fission to complete, which nicely coincides with experimental observations²². Without disassembly or rearrangement, our simulations suggest that the cylindrical micellar state is a stable or at least long-lived structure, that impedes further topological transitions.

Acknowledgments

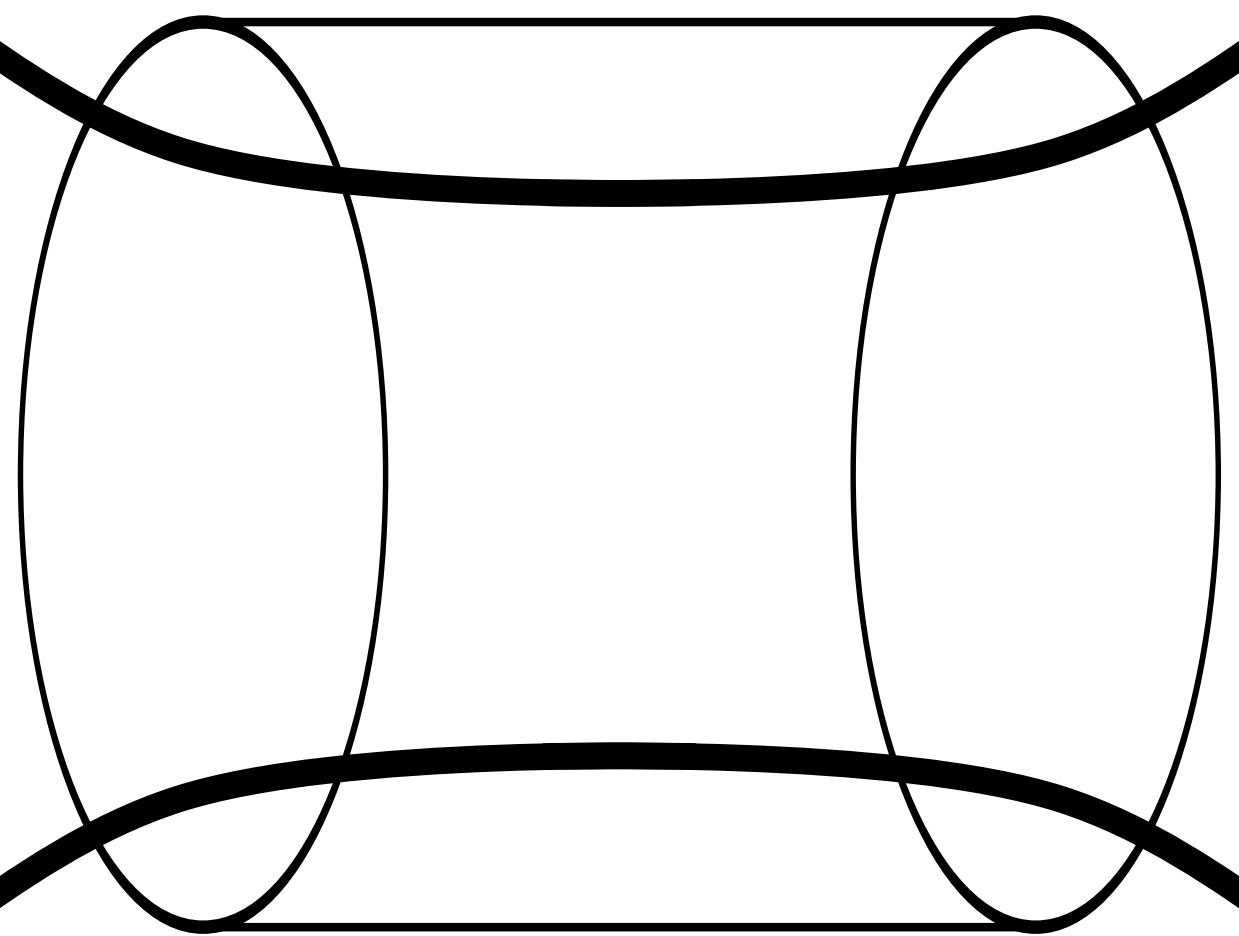
It is a great pleasure to thank Vadim A. Frolov for stimulating discussion. Financial support by the Volkswagen foundation and the CRC 803 "Functionality controlled by organization in and between membranes" (B03) as well as generous computing time at the HLRN Hannover/Berlin, the Jülich Supercomputer Center and the GWDG Göttingen are gratefully acknowledged.

References

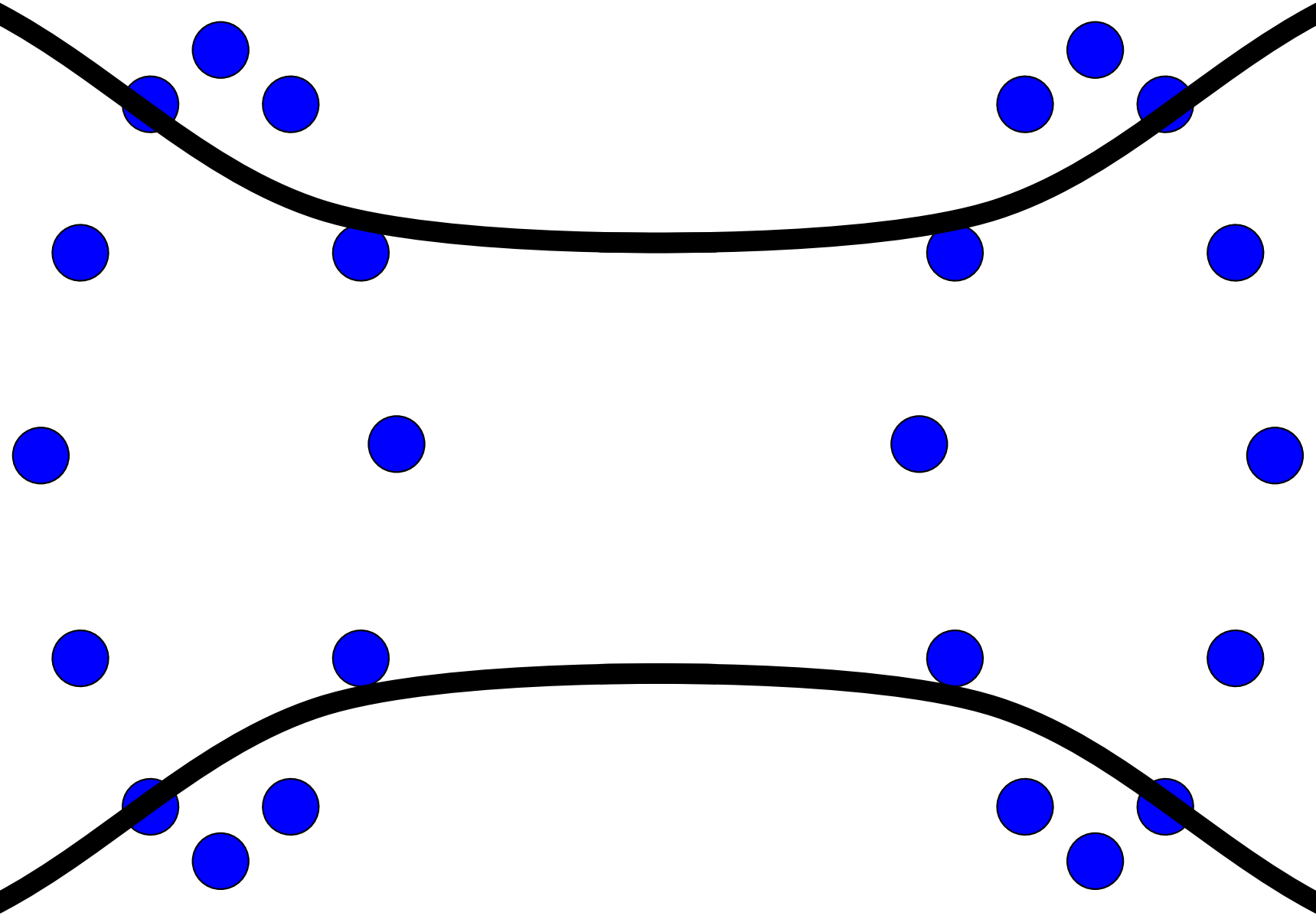
- 1 B. Alberts, D. Bray, J. Lewis, M. Raff, K. Roberts and J. D. Watson, *Molecular Biology of the Cell*, Garland, 4th edn, 2002.
- 2 Y. Kozlovsky and M. M. Kozlov, *Biophys. J.*, 2003, **85**, 85–96.
- 3 G. Fabrikant, S. Lata, J. D. Ricles, J. A. G. Briggs, W. Weissenhorn and M. M. Kozlov, *PLoS Comput. Biol.*, 2009, **5**, e1000575.
- 4 M. M. Kozlov, S. L. Leikin, L. V. Chernomordik, V. S. Markin and Y. A. Chizmadzhev, *Eur. Biophys. J.*, 1989, **17**, 121–129.
- 5 Y. Kozlovsky and M. M. Kozlov, *Biophys. J.*, 2002, **82**, 882–895.
- 6 M. Fuhrmans, G. Marelli, Y. G. Smirnova and M. Müller, *Chem. Phys. Lipids*, 2014.
- 7 A. M. van der Blik, T. E. Redelmeier, H. Damke, E. J. Tisdale, E. M. Meyerowitz and S. L. Schmid, *J. Cell Biol.*, 1993, **122**, 553–563.
- 8 J. S. Herskovits, C. C. Burgess, R. A. Obar and R. B. Vallee, *J. Cell Biol.*, 1993, **122**, 565–578.
- 9 H. Damke, T. Baba, D. E. Warnock and S. L. Schmid, *J. Cell Biol.*, 1994, **127**, 915–934.
- 10 A. B. Muhlberg, D. E. Warnock and S. L. Schmid, *EMBO J.*, 1997, **16**, 6676–6683.
- 11 D. D. Binns, B. Barylko, N. Grichine, M. A. L. Atkinson, M. K. Helms, D. M. Jameson, J. F. Eccleston and J. P. Albanesi, *J. Protein Chem.*, 1999, **18**, 277–290.
- 12 J. E. Hinshaw and S. L. Schmid, *Nature*, 1995, **374**, 190–192.
- 13 J. F. Carr and J. E. Hinshaw, *J. Biol. Chem.*, 1997, **272**, 28030–28035.
- 14 K. Takei, P. S. McPherson, S. L. Schmid and P. De Camilli, *Nature*, 1995, **374**, 186–190.
- 15 S. M. Sweitzer and J. E. Hinshaw, *Cell*, 1998, **93**, 1021–1029.
- 16 D. Danino, K. H. Moon and J. E. Hinshaw, *J. Struct. Biol.*, 2004, **147**, 259–267.
- 17 M. H. B. Stowell, B. Marks, P. Wigge and H. T. McMahon, *Nature Cell Biol.*, 1999, **1**, 27–32.
- 18 A. Roux, K. Uyhazi, A. Frost and P. De Camilli, *Nature*, 2006, **441**, 528–531.
- 19 M. Lenz, J. Prost and J. F. Joanny, *Phys. Rev. E*, 2008, **78**, 011911.

-
- 20 S. L. Schmid and V. A. Frolov, *Annu. Rev. Cell Dev. Biol.*, 2011, **27**, 79–105.
- 21 S. Sever, A. B. Muhlberg and S. L. Schmid, *Nature*, 1999, **398**, 481–486.
- 22 P. V. Bashkirov, S. A. Akimov, A. I. Evseev, S. L. Schmid, J. Zimmerberg and V. A. Frolov, *Cell*, 2008, **135**, 1276–1286.
- 23 T. J. Pucadyil and S. L. Schmid, *Cell*, 2008, **135**, 1263–1275.
- 24 A. V. Shnyrova, P. V. Bashkirov, S. A. Akimov, T. J. Pucadyil, J. Zimmerberg, S. L. Schmid and V. A. Frolov, *Science*, 2013, **339**, 1433–1436.
- 25 K. M. Ferguson, M. A. Lemmon, J. Schlessinger and P. B. Sigler, *Cell*, 1994, **79**, 199–209.
- 26 A. K. Downing, P. C. Driscoll, I. Gout, K. Salim, M. J. Zvelebil and M. D. Waterfield, *Curr. Biol.*, 1994, **4**, 884–891.
- 27 K. N. J. Burger, R. A. Demel, S. L. Schmid and B. de Kruijff, *Biochem.*, 2000, **39**, 12485–12493.
- 28 J. Zheng, S. M. Cahill, M. A. Lemmon, D. Fushman, J. Schlessinger and D. Cowburn, *J. Mol. Biol.*, 1996, **255**, 14–21.
- 29 M. G. J. Ford, S. Jenni and J. Nunnari, *Nature*, 2011, **477**, 561–566.
- 30 M. Hömberg and M. Müller, *J. Chem. Phys.*, 2010, **132**, 155104.
- 31 M. Fuhrmans and M. Müller, *Langmuir*, 2013, **29**, 4335–4349.
- 32 M. Hömberg and M. Müller, *EPL*, 2012, **97**, 68010.
- 33 M. Müller, K. Katsov and M. Schick, *Phys. Rep.*, 2006, **434**, 113–176.
- 34 S. J. Marrink, A. H. de Vries and D. P. Tieleman, *Biochim. Biophys. Acta, Biomembr.*, 2009, **1788**, 149–168.
- 35 A. J. Markvoort and S. J. Marrink, *Curr. Top. Membr.*, 2011, **68**, 259–294.
- 36 E. Boucrot, A. Pick, G. Camdere, N. Liska, E. Evergren, H. T. McMahon and M. M. Kozlov, *Cell*, 2012, **149**, 124–136.
- 37 K. C. Daoulas and M. Müller, *Adv. Polym. Sci.*, 2010, **224**, 197–233.
- 38 P. Warren and P. Espanol, *EPL (Europhys. Lett.)*, 1995, **30**, 191196.
- 39 S. Y. Trofimov, E. L. F. Nies and M. A. J. Michels, *J. Chem. Phys.*, 2005, **123**, 144102.
- 40 A. Roux, G. Koster, M. Lenz, B. Sorre, J. B. Manneville, P. Nassoy and P. Bassereau, *Proc. Natl. Acad. Sci. U. S. A.*, 2010, **107**, 4141–4146.
- 41 J. A. Mears, P. Ray and J. E. Hinshaw, *Structure*, 2007, **15**, 1190–1202.
- 42 N. Mehrotra, J. Nichols and R. Ramachandran, *Mol. Biol. Cell*, 2014, **25**, 879–890.
- 43 Y. Liu, S. Neumann, R. Ramachandran, S. M. Ferguson, T. J. Pucadyil and S. L. Schmid, *Proc. Natl. Acad. Sci. U. S. A.*, 2011, **108**, E234–E242.
- 44 P. E. MacDonald, L. Eliasson and P. Rorsman, *J. Cell Sci.*, 2005, **118**, 5911–5920.
- 45 J. María Cabeza, J. Acosta and E. Alés, *Traffic*, 2010, **11**, 1579–1590.
- 46 N. Mizuno, C. C. Jao, R. Langen and A. C. Steven, *J. Biol. Chem.*, 2010, **285**, 23351–23358.

A



B



C

